The climates of Earth's next supercontinent: effects of tectonics, rotation rate, and insolation

M. J. Way[1,2,3], H. S. Davies[4,5], J. C. Duarte[4,5,6], and J. A. M. Green[7]

[1]NASA Goddard Institute for Space Studies, New York, USA
[2]Goddard Space Flight Center Sellers Exoplanet Environments Collaboration
[3]Theoretical Astrophysics, Department of Physics and Astronomy, Uppsala University, Uppsala, Sweden
[4]Instituto Dom Luiz (IDL), Faculdade de Ciências, Universidade de Lisboa, Lisbon, Portugal
[5]Departamento de Geologia, Faculdade de Ciências, Universidade de Lisboa, Lisbon, Portugal
[6]School of Earth, Atmosphere and Environment, Monash University, Melbourne, Victoria, Australia
[7]School of Ocean Sciences, Bangor University, Menai Bridge, UK

Key Points:

- The climate of a distant future Earth is modeled for two different supercontinent scenarios.
- The latitudinal location of the supercontinents are critical to mean surface temperatures.

Corresponding author: Michael Way, michael.way@nasa.gov

Abstract

We explore two possible Earth climate scenarios, 200 and 250 million years into the future, using knowledge of the evolution of plate tectonics, solar luminosity, and rotation rate. In one scenario, a supercontinent forms at low latitudes, whereas in the other it forms at high northerly latitudes with an antarctic subcontinent remaining at the south pole. The climates between these two end points are quite stark, with differences in mean surface temperatures approaching 4 degrees. The fractional habitability (mean surface temperatures remaining between 0<T<100° year round) on land is shown to differ as much as 40% between the two simulations. These results demonstrate the need to consider alternative boundary conditions when simulating Earth-like exoplanetary climates.

Plain Language Summary

We investigate two tantalizing Earth climate scenarios 200 and 250 million years into the future. We show the role played by plate tectonics, the sun's increase in brightness, and a slightly slower rotation rate in these future climate scenarios. In one case the present day continents form into a single land-mass near the equator, and in the other case Antarctica stays put, but the rest of the present day continents are mostly pushed well north of the equator. The difference in the mean surface temperatures of these two cases differ up to 4 degree Celsius, while also being distinct in the total surface area in which they maintain temperatures allowing liquid water to exist year round.

1 Introduction

Earth's near-future climate has been extensively explored via the IPCC and associated CMIP studies (e.g. Collins et al., 2013). Earth's ancient climate has also been studied at various levels of detail, including the Cretaceous greenhouse (e.g., Huber et al., 2018), the Neoproterozoic Snowball (Pierrehumbert et al., 2011), and on the supercontinent Pangea (e.g., Parrish, 1993). Earth's deep time future is a novel research discipline, and changes in deep-time future climate, induced by changes in topography and land/sea masks (e.g., Davies et al., 2018), have yet to be explored until now.

The geological formations on the ever-changing surface of the Earth have a strong influence on our climate. The separation of Australia from Antarctica (DeConto & Pollard, 2003) and the opening of the Drake Passage (Barker, 2001) 30–40 million years ago induced the Antarctic glaciation. The development of the Caribbean arc and closing of the Panama Isthmus allowed the Gulf Stream to form, with major consequences for global climate (Montes et al., 2015). A closure of the Strait of Gibraltar led to the Messinian Salinity Crisis (Krijgsman et al., 1999), whereas the Himalayas, a consequence of the India-Eurasia collision, allows for the monsoon (Tada et al., 2016). Recently, Farnsworth et al. (2019) showed that the climate sensitivity for the period 150–35 million years ago is dependent on the continental configuration, particularly ocean area. Schmittner et al. (2011) investigated the effects of mountains on ocean circulation patterns of present day Earth and concluded that the current configuration of mountains and ice sheets determines the relative deep-water formation rates between the Atlantic and the Pacific Oceans.

The tectonic plates on Earth aggregate into supercontinents and then disperse on a cycle of 400-600 million years – the supercontinent cycle (Davies et al., 2018; Pastor-Galán et al., 2019; Yoshida, 2016; Yoshida & Santosh, 2018). The latest supercontinent, Pangea, formed around 310 million years ago, and started breaking up around 180 million years ago. The next supercontinent will most likely form in 200–250 million years, meaning Earth is currently about halfway through the scattered phase of the current supercontinent cycle (Davies et al., 2018).

There are obvious and strong links between large scale tectonics and climate. It would be interesting to know what Earth's climate could be like in the distant future, when continental movements have taken Earth away from the current continental configuration (Davies et al., 2018). This will be explored here, where we investigate what the climate may look like on Earth in a future supercontinent state. A secondary application of climate modelling of the deep-time future is to create a climate model of an Earth-like exoplanet using the parameters known to sustain habitability and a stable biosphere (Earth). Using the Deep-time future Earth as a basis for exoplanetary climate studies allows us to establish sensitivity ranges for the habitability and climate stability of the future Earth and its distant cousins in our Milky Way Galaxy.

2 Methods

2.1 Tectonic maps

Maps of the future Earth were produced based on two plausible scenarios for future Earth: Aurica (forming around 250 million years from now; see Duarte et al., 2018) and Amasia (forming around 200 million years from now; Mitchell et al., 2012) – see Davies et al. (2018) for a summary. In both cases the ocean bathymetry was kept as in Davies et al. (2019), with continental shelf seas 150 m deep, mid-ocean ridges 1600 m deep at the crest point and deepening to the abyssal plains within 5°, and subduction zones 6000 m deep. The abyssal plain was set to a depth maintaining the present day ocean volume. Each topographic file was generated with a 1/4° horizontal resolution in both latitude and longitude.

We generated three subsets of maps for each of the two supercontinent scenarios (see Table 1):

1. Low mean topography (land close to sea level), with no mountains (CTRL)
2. Higher mean topography (land close to present day mean topography) with no mountains (PD)
3. Low topography with mountains (land close to sea level interspersed with mountains) (MTNS)

The first subset of maps serve as a control (CTRL), allowing us to test the effect of the position and geometry of the continents without the influence of high topographies and particular features such as mountain ranges. It could also simulate a supercontinent that has existed long enough to have been almost fully eroded. The land here has been assigned topography with a normal distribution (mean = 1 m and standard deviation = 50 m), giving topographic heights varying from 1 to 200 m.

The second set of maps assume mean topographic values close to those of present day (PD) but with no significant variation (e.g., no high mountains). This was made by applying a random topography following a normal distribution with mean and standard deviations closer to those of present day Earth's topography (i.e., mean of 612 m and standard deviation of 712 m). The resulting topography varies between 1 and 4000 m in height.

In the third set (MTNS), we included mountain ranges. The land of the supercontinent was first given a random topography similar to the control map (varying randomly between 1 and 200 m), after which mountains were added manually. The mountains are of three types: 1) Himalaya-type, which result from the collision of continents during the formation of the supercontinent, with an average peak elevation of 7500 m; 2) Andes-type, located at the margins of the continents along major subduction zones, with an average peak elevation of 4000 m; and 3) Appalachian-type, which correspond to eroded orogens that were formed and then partially eroded during the supercontinent cycle, with

Table 1. A summary list of the simulations & results.

Sim	Name	Topography	I[a]	LoD[b]	Runtime (years)	T[c] (C)	Balance (Wm^{-2})	A[d] (%)	SnowFr[e] (%)
				Aurica					
01	Aurica_Rand_CTRL	CTRL	1.0260	24.5	2000	20.5	0.23	30.5	0.5
02	Aurica_Rand_PD	PD	”	24.5	2500	20.6	0.10	30.1	0.6
03	Aurica_250f	MTNS	”	24.5	2000	20.6	0.20	30.3	1.5
				Amasia					
04	Amasia_Rand_CTRL	CTRL	1.0223	24.5	2567	19.7	0.42	30.1	4.2
05	Amasia_Rand_PD	PD	”	24.5	3000	17.2	0.25	31.1	9.0
06	Amasia_200f	MTNS	”	24.5	3000	20.2	0.24	30.0	4.7
				Earth					
07	Earth_noAer_noO3	–	1.0	24.0	1000	14.2	0.17	31.1	11.1

[a] Insolation, where 1.0 = 1361 W m^{-2} (Modern Earth).
[b] LoD = Length of Day in hours.
[c] Global mean surface temperature in degrees Celsius from an average over the last 10 years of the model run.
[d] Planetary Albedo.
[e] Snow and Ice, global fractional area.

an average peak elevation of 2000 m. In all cases, the width of the mountains is 5° from peak to base.

2.2 Rotation changes

Day-length for the future was computed based on the simulated tidal dissipation rates presented in Green et al. (2018). The tidal dissipation rates at the supercontinent state is only about 20% of that at present, leading to a change in day length that cannot be ignored. The time rate of change in Earth's angular rotation rate, $d\Omega/dt$, can be approximated by (MacDonald, 1964)

$$\frac{d\Omega}{dt} = \frac{45}{8} k \frac{G m^2 A^3}{M r^6} \sin(2\alpha) \tag{1}$$

Here $k = 0.2$ is a Love number, $G = 6.67 \times 10^{-11}$ m^3 kg^{-1} s^{-2} is the gravitational constant, $m = 7.3 \times 10^{22}$ kg is the moon's mass, $M = 6 \times 10^{24}$ kg is the Earth's mass, $A = 6.4 \times 10^6$ m is Earth's mean radius, $r = 3.8 \times 10^8$ m is the Earth-moon distance, and is the angle (α) between the tidal bulge and the Earth-moon center line. The latter is defined from $\sin(2\alpha) = D/W$, i.e., the ratio between the tidal dissipation rate D and the work done by the tide generating force, W; both are computed by the numerical tidal model used in Green et al. (2018).

The resulting spin down is $d\Omega/dt = 2.23 \times 10^{-22}$ s^{-2}, or the equivalent of a lengthening of a day by 0.5 hours over 200 million years (My). This length of day (24.5 hours) was consequently used in the General Circulation Model simulations discussed below.

2.3 General Circulation Model set up

The ROCKE-3D General Circulation Model (GCM) version Planet_1.0 (R3D1) as described in Way et al. (2017) is utilized for this study. A fully coupled dynamic ocean is utilized. Data from Claire et al. (2012) (see their Table 2) is used to estimate the solar flux $\sim$ 250 My into the future impinging upon Earth. We do not change the solar spectrum as the changes for such a small leap into the future will be minimal in terms of its effect on Earth's atmosphere. We use an insolation value of 1.019 estimated as the mean of today's value of 1 and the value 500 My into the future of 1.037 from Claire et al. (2012). Hence the insolation in W m^{-2} is 1361 x 1.019 = 1397 W/m^{-2}.

We use a 50/50 clay/sand mix for the soil given that we have no constraints on what the surface will be like in the deep future and is a value commonly used in the exoplanet community (e.g. Yang et al., 2014; Way et al., 2018). 40 cm of water is initially distributed into each soil grid cell. We use a ground albedo of 0.2 at model start, but the albedo will change via snow deposition (brighter), or from rainfall (darker) as the GCM moves forward in time.

The original topography resolution of 1/4°×1/4° from the tectonic maps discussed in Section 2.1 is down-sampled to a resolution of 4°×5° in latitude by longitude, which is the default R3D1 resolution. The standard deviation from the down-sampling is used to set the roughness length of the surface in each grid cell. River flow direction is based on the resulting topography and exits to the ocean when possible. Large inland seas (typically less than 15 contiguous grid cells) are defined as lakes rather than ocean grid cells. The GCM allows lakes to expand and contract as dictated by the competition between evaporation and precipitation. The same holds for the possible creation and disappearance of lakes. This allows the model to handle inland surface water in a more sophisticated manner than making all surface water defined as ocean grid cells. This is highly desirable because ocean grid cells cannot be created or destroyed during a model run.

Any ocean grid cell with a depth less than 150 meters (from the down-sampled 4°× 5° data) was set to have a value of 204 meters (the mean depth of ocean model level 6). This is especially important at high latitudes where the ocean may freeze to the bottom, which will cause the model to crash due to its inability to dynamically change surface types from ocean to land ice.

The down-sampling has a side effect in that the land-sea mask will differ slightly between the three topographic types (CTRL, PD, MTNS). For example, in a case with a collection of ocean or lake grid cells adjacent to a number of high elevation land topography grid cells the down-sampling may change the combined ocean + land grid cells into a land grid cell, or vice-versa if the mean of the ocean grid cells is larger than that of the land grid cells. This is why the land/sea masks differ between CTRL, PD and MTNS in Figure 1, even though their 1/4°×1/4° parents had exactly the same land-sea mask.

The atmosphere is set to roughly Earth constituents in the year 1850: Nitrogen dominated with 21% Oxygen, 285 ppmv CO_2, 0.3 ppmv N_2O, and 0.79 ppmv CH_4. No aerosols or Ozone (O_3) are included. For comparison purposes we include a modern Earth-like land/sea mask (Simulation 07: Earth_noAer_noO3) with these same atmospheric constituents, but with modern insolation (1361 W m^{-2}) and a bathtub ocean. The Earth-like land/sea mask is described in Way et al. (2018) and shown in Figure 8 of that paper.

3 Results

Previous work has shown that ancient Earth supercontinent phases, which are comparable to our Aurica Simulations 01-03, have had more arid interiors where weathering effects and CO_2 draw down may have been less efficient (e.g. Jellinek et al., 2019). This would increase surface temperatures as the balance of CO_2 would tend to be larger than present day because volcanic outgassing (sources) would likely remain constant while CO_2 drawdown (sinks) would decrease. However, there are other climatic effects to consider. For example, the Amasia reconstruction is essentially an arctic supercontinent with an independent and isolated antarctic continent, meaning both poles are covered by land, and much of that is covered by ice. Amasia is thus in essence a shift to consolidate the present day domination of northern latitude land masses even further north.

This increase in land masses at northerly latitudes means that there is less ocean heat transport to melt the ice in the northern hemisphere summers. Consequently, more ice resides on land and in lakes all year round near the north pole, as we see in present

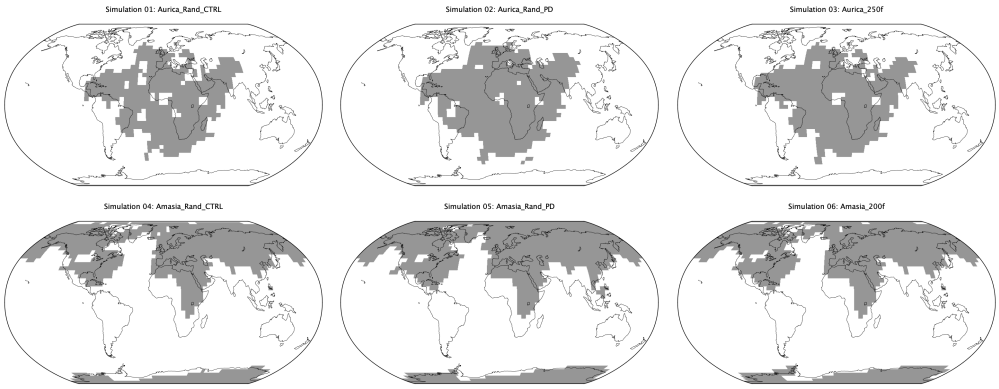

Figure 1. Land (grey) and Sea (white) masks used in experiments of Table 2.1. Present day Earth continental outlines are shown for reference.

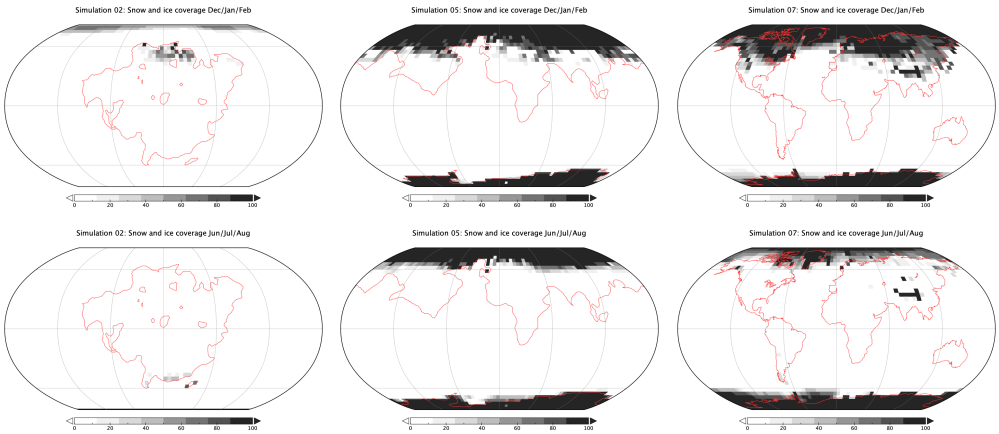

Figure 2. Individual grid cell snow+ice fractional amounts. For Simulation 02 (left), Simulation 05 (middle) and Simulation 07 (right) for a sum of the months of December, January and February (top) and June, July and August (bottom) in the last year of each simulation.

day Antarctica. This is the well known ice-albedo climate feedback and explains why these simulations tend to be cooler than the others. The coolest simulation is Simulation 05 (Amasia_Rand_PD), because it has very very few inland seas in the north (compared to Simulations 04 & 06) that could thaw out in the summers, as well as less ocean area at high latitudes to transport heat. Hence, it tends to remain cooler than Simulations 04 & 06 with similar land/sea masks (see Figure 1).

It is informative to contrast Simulation 02 (Aurica_Rand_PD) with Simulation 05 (Amasia_Rand_PD). Simulation 02 is more contiguous (less inland lakes & seas), has land at lower latitudes and uses the same "present day" (PD) topographic values for inputs as Simulation 05. Simulation 05 also has contiguous land, but at much higher latitudes. In Table 2.1 we give their mean surface temperatures, planetary albedo and fractional snow & ice coverage. The snow & ice coverage in particular is clearly the biggest climatic factor as shown in Figure 2. There, we show the seasonal snow & ice coverage for Simulations 02 & 05 where Dec/Jan/Feb is an average over northern hemisphere winter months December, January & February. Jun/Jul/Aug is an average over the northern hemisphere summer months of June, July & August. We could have used albedo, but it is an imperfect measure here since in the northern winter months much of the area above the

Arctic circle gives null values (no reflected light, hence no albedo) and the same during the southern winter months for land areas below the Antarctic circle. Regardless, in Table 2.1 it is clear that the snow & ice fractions are much higher for the Amasia runs (04, 05, 06) compared to the other three Aurica runs (01, 02, 03), and highest for Simulation 05 in particular. The higher snow fraction amount of Simulation 05 corresponds directly to the lower surface temperature in this set of runs. This coldest of the future climates (Simulation 05) has a similar global 10 year mean albedo to that of Simulation 07 (Earth). However, the Earth simulation is cooler because it has more snow & ice at high northerly latitudes and has a lower insolation.

The general effect of the different land/sea masks between Simulations 01–03 and 04–06 and how they compare with modern Earth in Simulation 07 are seen in Supplementary Material Figures S1 and S2. In Figure S1 we plot the stream function which indicates the strength of the Hadley circulation. While the Amasia stream function is roughly the same as modern day Earth's, the Aurica stream function is about an order of magnitude weaker. Surely this is due to the large super continent at low latitudes in the Aurica simulation that prevent moisture uptake at these lower latitudes.

On the other hand in Figure S2 we plot the Atmospheric, Oceanic and Total (Atmospheric + Ocean) meridional heat transport in units of petawatts. Simulations 01–03 (Aurica) and 07 (Earth) are decidedly similar, while that of Amasia appears to be generally stronger. The largest differences are the ocean transport in the middle figures where the low latitude landmass of Aurica prevents large meridional flows, whereas the lack of low-latitude landmasses in Simulations 04–06 (Amasia) allow for greater transport. Similar contrasts were seen in ancient Venus simulations at the inner edge of the habitable zone (Way et al., 2016) where a land-sea mask with more land at lower latitudes, versus modern Earth, generated distinct global mean surface temperatures.

We were not able to discern any marked differences in climate due to the day length being 30 minutes longer. This was examined by looking at the difference between Simulation 07, which uses a modern Earth day length, and the same simulation (unpublished) using the same day length as Simulations 01–06. So, any differences between Simulations 01–06 and Simulation 07 mentioned above are likely to due to differences in land-sea mask, insolation, and associated climate dynamics.

Work by Spiegel et al. (2008) uses a metric of "climatic habitability" that defines the amount of surface area of a planet that can host liquid water (e.g., surface temperatures in the range $0<T<100°C$) at modern Earth atmospheric pressures. Again focusing on Simulation 02 and 05 we find that Simulation 02 has much less fractional habitability if we look at land and lakes – 58% – compared with Simulation 05 (99.8%). Sea surface temperatures are more balanced: Simulation 02 was at 73% and Simulation 05 was at 71% habitability for the ocean. These numbers are all taken from averages of the last 10 years of each run.

4 Conclusions

The supercontinents of the future can provide us some guidance on how surface temperatures will increase or decrease depending on how the continents are distributed. But there are other factors to consider related to weathering rates and volcanic outgassing (e.g. Jellinek et al., 2019), not to mention the related role of atmospheric pressure (Gaillard & Scaillet, 2014).

As mentioned above, the small 30 minute decrease in rotation rate for Simulations 01–06 as compared with modern Earth (Simuation 07) appears to play little or no role in the climate dynamics as there is no discernible difference in the strength or distribution of the Hadley/Ferrell/Polar cells when comparing Simulation 05 and Simulation 07

(see Figure S2). There is a decrease in the strength of Simulation 02 compared to 07 (Figure S2), but this is likely due to the large low latitude supercontinent in Simulation 02.

While we discuss the future climate of Earth we do not touch on the future of life. There are too many uncertainties for us to speculate, but recent work provides some guidelines (Mello & Friaça, 2019). The reduced tides during the supercontinent stage (Davies et al., 2019) will lead to reduced vertical mixing rates, i.e. a reduced vertical diffusivity in the abyssal ocean (Munk, 1966; Wunsch & Ferrari, 2004). This may have implications for ocean ecosystems, and biodiversity. At the same time it appears that the formation of Pangea had little effect on the global biodiversity of marine animals (Zaffos & Peters, 2017) and Pangea was in a very weak tidal state (Green et al., 2017).

It would be interesting to compare the GCM derived climates for the supercontinent at low latitude in the Aurica runs with previous work on Pangea (e.g. Chandler et al., 1992; Chandler, 1994; Fluteau et al., 2001; Gibbs et al., 2002; Roscher et al., 2011). Unfortunately it is difficult to make a proper comparison for a number of reasons. First, all of these previous works use either atmosphere only GCMs (i.e., no ocean) or shallow mixed layer oceans with either prescribed horizontal heat transport or none at all. Secondly, unlike Aurica, Pangea spanned not only lower latitudes (like Aurica), but also high southern latitudes where ice/snow forms easily (e.g. Chandler et al., 1992, see Figure 5). Finally, there are different reconstructions for different time periods and not all are directly comparable to those we simulate herein. This makes a direct comparison with Pangea complicated and we leave such an analysis for the future.

These new reconstructions may prove useful for exoplanetary studies where researchers will have a larger library of topographies and land/sea masks to chose from when estimating the probability of surface habitability on neighboring worlds.

Acknowledgments

Thanks goes to Jeffrey Jonas at The Goddard Institute for Space Studies for his help with the map overlays in Figure 2. This work was supported by NASA's Nexus for Exoplanet System Science (NExSS). Resources supporting this work were provided by the NASA High-End Computing (HEC) Program through the NASA Center for Climate Simulation (NCCS) at Goddard Space Flight Center. MJW acknowledges support from the GSFC Sellers Exoplanet Environments Collaboration (SEEC), which is funded by the NASA Planetary Science Division's Internal Scientist Funding Model. HSD acknowledges funding from FCT (ref. UID/GEO/50019/2019—Instituto Dom Luiz; FCT PhD grant ref. PD/BD/135068/2017). JCD acknowledges an FCT Researcher contract, an exploratory project grant ref. IF/00702/2015, and the FCT project UID/GEO/50019/2019-IDL. JAMG acknowledges funding from NERC, grant NE/S009566/1 (MATCH). All GCM NetCDF data used in this publication can be downloaded from the NCCS data portal:

https://portal.nccs.nasa.gov/GISS_modelE/ROCKE-3D/publication-supplements/

References

Barker, P. F. (2001). Scotia sea regional tectonic evolution: implications for mantle flow and palaeocirculation. *Earth-Science Reviews*, *55*, 1-39.

Chandler, M. A. (1994, 01). Depiction of modern and Pangean deserts: Evaluation of GCM hydrological diagnostics for paleoclimate studies. In *Pangea: Paleoclimate, Tectonics, and Sedimentation During Accretion, Zenith, and Breakup of a Supercontinent*. Geological Society of America. Retrieved from `https://doi.org/10.1130/SPE288-p117` doi: 10.1130/SPE288-p117

Chandler, M. A., Rind, D., & Ruedy, R. (1992, 05). Pangaean climate during the Early Jurassic: GCM simulations and the sedimentary record of paleoclimate. *GSA Bulletin*, *104*(5), 543-559. Retrieved from `https://`

doi.org/10.1130/0016-7606(1992)104<0543:PCDTEJ>2.3.CO;2 doi: 10.1130/0016-7606(1992)104⟨0543:PCDTEJ⟩2.3.CO;2

Claire, M. W., Sheets, J., Cohen, M., Ribas, I., Meadows, V. S., & Catling, D. C. (2012, September). The Evolution of Solar Flux from 0.1 nm to 160 μm: Quantitative Estimates for Planetary Studies. *Astrophysical Journal*, *757*, 95. doi: 10.1088/0004-637X/757/1/95

Collins, M., Knutti, R., Arblaster, J., Dufresne, J.-L., Fichefet, T., Friedlingstein, P., ... Wehner, M. (2013). Long-term Climate Change: Projections, Commitments and Irreversibility. *Climate Change 2013: The Physical Science Basis. Contribution of Working Group I to the Fifth Assessment Report of the Intergovernmental Panel on Climate Change*, 1029–1136. doi: 10.1017/CBO9781107415324.024

Davies, H. S., Green, J. A. M., & Duarte, J. C. (2018). Back to the future: Testing different scenarios for the next supercontinent gathering. *Global Planetary Change*, *169*, 133–144.

Davies, H. S., Green, J. A. M., & Duarte, J. C. (2019). Back to the future ii: Tidal evolution of four supercontinent scenarios. *Earth System Dynamics*, submitted.

DeConto, R. M., & Pollard, D. (2003). Rapid Cenozoic glaciation of Antarctica induced by declining atmospheric CO2. *Nature*, *421*, 245–249.

Duarte, J. C., Schellart, W. P., & Rosas, F. M. (2018). The future of Earth's oceans: Consequences of subduction initiation in the Atlantic and implications for supercontinent formation. *Geological Magazine*, *155*(1), 45–58. doi: 10.1017/S0016756816000716

Farnsworth, A., Lunt, D., O'Brien, C., Foster, G., Inglis, G., Markwick, P., ... Robinson, S. (2019). Climate sensitivity on geological timescales controlled by non-linear feedbacks and ocean circulation. *Geophysical Research Letters*, 2019GL083574.

Fluteau, F., Besse, J., Broutin, J., & Ramstein, G. (2001). The late permian climate. what can be inferred from climate modelling concerning pangea scenarios and hercynian range altitude? *Palaeogeography, Palaeoclimatology, Palaeoecology*, *167*(1), 39 - 71. Retrieved from http://www.sciencedirect.com/science/article/pii/S0031018200002303 doi: https://doi.org/10.1016/S0031-0182(00)00230-3

Gaillard, F., & Scaillet, B. (2014, Oct). A theoretical framework for volcanic degassing chemistry in a comparative planetology perspective and implications for planetary atmospheres. *Earth and Planetary Science Letters*, *403*, 307-316. doi: 10.1016/j.epsl.2014.07.009

Gibbs, M. T., Rees, P. M., Kutzbach, J. E., Ziegler, A. M., Behling, P. J., & Rowley, D. B. (2002). Simulations of permian climate and comparisons with climate-sensitive sediments. *The Journal of Geology*, *110*(1), 33-55. Retrieved from https://doi.org/10.1086/324204 doi: 10.1086/324204

Green, J. A. M., Huber, M., Waltham, D., Buzan, J., & Wells, M. (2017). Explicitly modelled deep-time tidal dissipation and its implication for lunar history. *Earth and Planetary Science Letters*, *461*, 46–53. doi: 10.1016/j.epsl.2016.12.038

Green, J. A. M., Molloy, J. L., Davies, H. S., & Duarte, J. C. (2018). Is there a tectonically driven supertidal cycle? *Geophysical Research Letters*, *45*, 3568–3576. doi: 10.1002/2017GL076695

Huber, B. T., MacLeod, K. G., Watkins, D. K., & Coffin, M. F. (2018). The rise and fall of the cretaceous hot greenhouse climate. *Global and Planetary Change*, *167*, 1 - 23. doi: https://doi.org/10.1016/j.gloplacha.2018.04.004

Jellinek, M., Lenardic, A., & Pierrehumbert, R. (2019, 06). Ice, fire or fizzle: The climate footprint of earth's supercontinental cycles. *Geochemistry, Geophysics, Geosystems*, 10.

Krijgsman, W., Hilgen, F. J., Raffi, I., Sierro, F. J., & Wilson, D. S. (1999). Chronology, causes and progression of the Messinian salinity crisis. *Nature*, *400*(6745), 652–655.

MacDonald, G. J. F. (1964, 8). Tidal friction. *Reviews of Geophysics*, *2*(3), 467–541. Retrieved from `https://doi.org/10.1029/RG002i003p00467` doi: 10.1029/RG002i003p00467

Mello, F. d. S., & Friaça, A. C. S. (2019). The end of life on earth is not the end of the world: converging to an estimate of life span of the biosphere? *International Journal of Astrobiology*, 1-18. doi: 10.1017/S1473550419000120

Mitchell, R. N., Kilian, T. M., & Evans, D. A. D. (2012). Supercontinent cycles and the calculation of absolute palaeolongitude in deep time. *Nature*, *482*, 208–211.

Montes, C., Cardona, A., Jaramillo, C., Pardo, A., Silva, J. C., Valencia, V., ... Niño, H. (2015). Middle Miocene closure of the Central American Seaway. *Science*, *348*, 226–229.

Munk, W. H. (1966). Abyssal recipes. *Deep-Sea Research and Oceanographic Abstracts*, *13*(4), 707–730. doi: 10.1016/0011-7471(66)90602-4

Parrish, J. (1993, 03). Climate of the supercontinent pangea. *Journal of Geology*, *101*, 215-233. doi: 10.1086/648217

Pastor-Galán, D., Nance, R. D., Murphy, J. B., & Spencer, C. J. (2019). Supercontinents: myths, mysteries, and milestones. *Geological Society, London, Special Publications*, *470*(1), 39–64. Retrieved from `https://sp.lyellcollection.org/content/470/1/39` doi: 10.1144/SP470.16

Pierrehumbert, R. T., Abbot, D. S., Voigt, A., & Koll, D. (2011). Climate of the neoproterozoic. *Annual Reviews of Earth and Planetary Sciences*, 417-460.

Roscher, M., Stordal, F., & Svensen, H. (2011). The effect of global warming and global cooling on the distribution of the latest permian climate zones. *Palaeogeography, Palaeoclimatology, Palaeoecology*, *309*(3), 186 - 200. Retrieved from `http://www.sciencedirect.com/science/article/pii/S0031018211002987` doi: https://doi.org/10.1016/j.palaeo.2011.05.042

Schmittner, A., Silva, T. A. M., Fraedrich, K., Kirk, E., & Lunkeit, F. (2011). Effects of Mountains and Ice Sheets on Global Ocean Circulation. *Journal of Climate*, *24*, 2814–2829.

Spiegel, D. S., Menou, K., & Scharf, C. A. (2008, Jul). Habitable Climates. *Astrophysical Journal*, *681*(2), 1609-1623. doi: 10.1086/588089

Tada, R., Zheng, H., & Clift, P. D. (2016). Evolution and variability of the Asian monsoon and its potential linkage with uplift of the Himalaya and Tibetan Plateau. *Progress in Earth and Planetary Science*, *3*, 4.

Way, M. J., Aleinov, I., Amundsen, D. S., Chandler, M. A., Clune, T. L., Del Genio, A. D., ... Tsigaridis, K. (2017, July). Resolving Orbital and Climate Keys of Earth and Extraterrestrial Environments with Dynamics (ROCKE-3D) 1.0: A General Circulation Model for Simulating the Climates of Rocky Planets. *Astrophysical Journal Supplement Series*, *231*, 12. doi: 10.3847/1538-4365/aa7a06

Way, M. J., Del Genio, A. D., Aleinov, I., Clune, T. L., Robinson, T. D., Kelly, M., & Kiang, N. Y. (2018). Climates of warm earth-like planets. i. 3d model simulations. *The Astrophysical Journal Supplement Series*, *239*(2).

Way, M. J., Genio, A. D. D., Kiang, N. Y., Sohl, L. E., Grinspoon, D. H., Aleinov, I., ... Al, W. A. Y. E. T. (2016). Was Venus the first habitable world of our solar system? *Geophysical Research Letters*, *43*, 8376-8383.

Wunsch, C., & Ferrari, R. (2004). Vertical mixing, energy, and the general circulation of the oceans. *Annual Review of Fluid Mechanics*, *36*(1), 281–314.

Yang, J., Boué, G., Fabrycky, D. C., & Abbot, D. S. (2014). Strong dependence of the inner edge of the habitable zone on planetary rotation rate. *Astrophysical Journal Letters*, *787*(1). doi: 10.1088/2041-8205/787/1/L2

Yoshida, M. (2016, 09). Formation of a future supercontinent through plate motion–driven flow coupled with mantle downwelling flow. *Geology*, *44*(9), 755-758. Retrieved from https://doi.org/10.1130/G38025.1 doi: 10.1130/G38025.1

Yoshida, M., & Santosh, M. (2018). Voyage of the indian subcontinent since pangea breakup and driving force of supercontinent cycles: Insights on dynamics from numerical modeling. *Geoscience Frontiers*, *9*(5), 1279 - 1292. Retrieved from http://www.sciencedirect.com/science/article/pii/S1674987117301536 (SPECIAL ISSUE: Frontiers in geoscience:A tribute to Prof. Xuanxue Mo) doi: https://doi.org/10.1016/j.gsf.2017.09.001

Zaffos, S., A. Finneganb, & Peters, S. E. (2017). Plate tectonic regulation of global marine animal diversity. *PNAS*, *114*(22), 5653–5658. Retrieved from https://www.pnas.org/content/114/22/5653 doi: https://doi.org/10.1073/pnas.1702297114

fig2d.png.

Simulation 02: Snow and ice coverage Jun/Jul/Aug

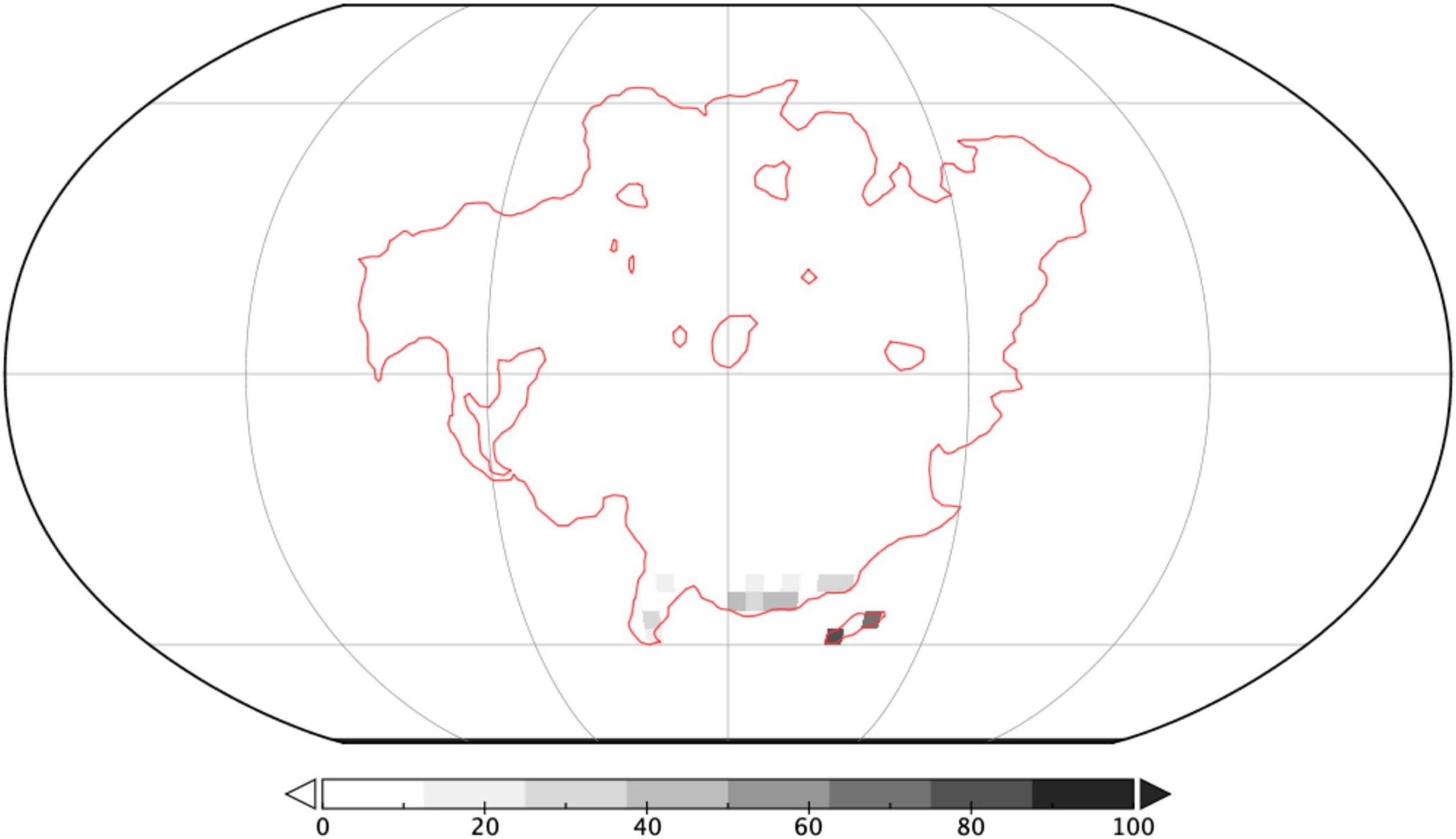

fig2e.png.

Simulation 05: Snow and ice coverage Jun/Jul/Aug

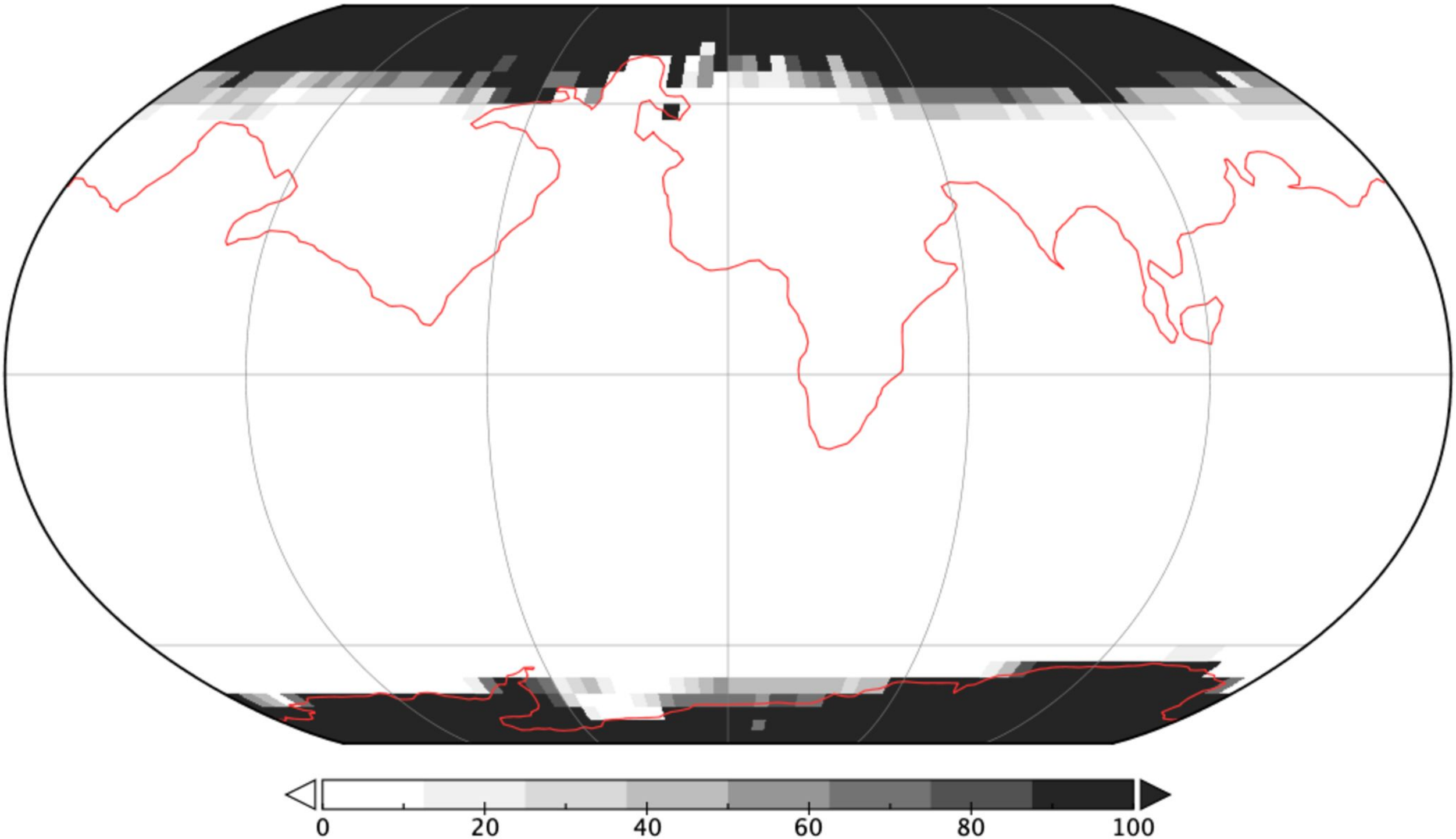

fig2f.png.

Simulation 07: Snow and ice coverage Jun/Jul/Aug

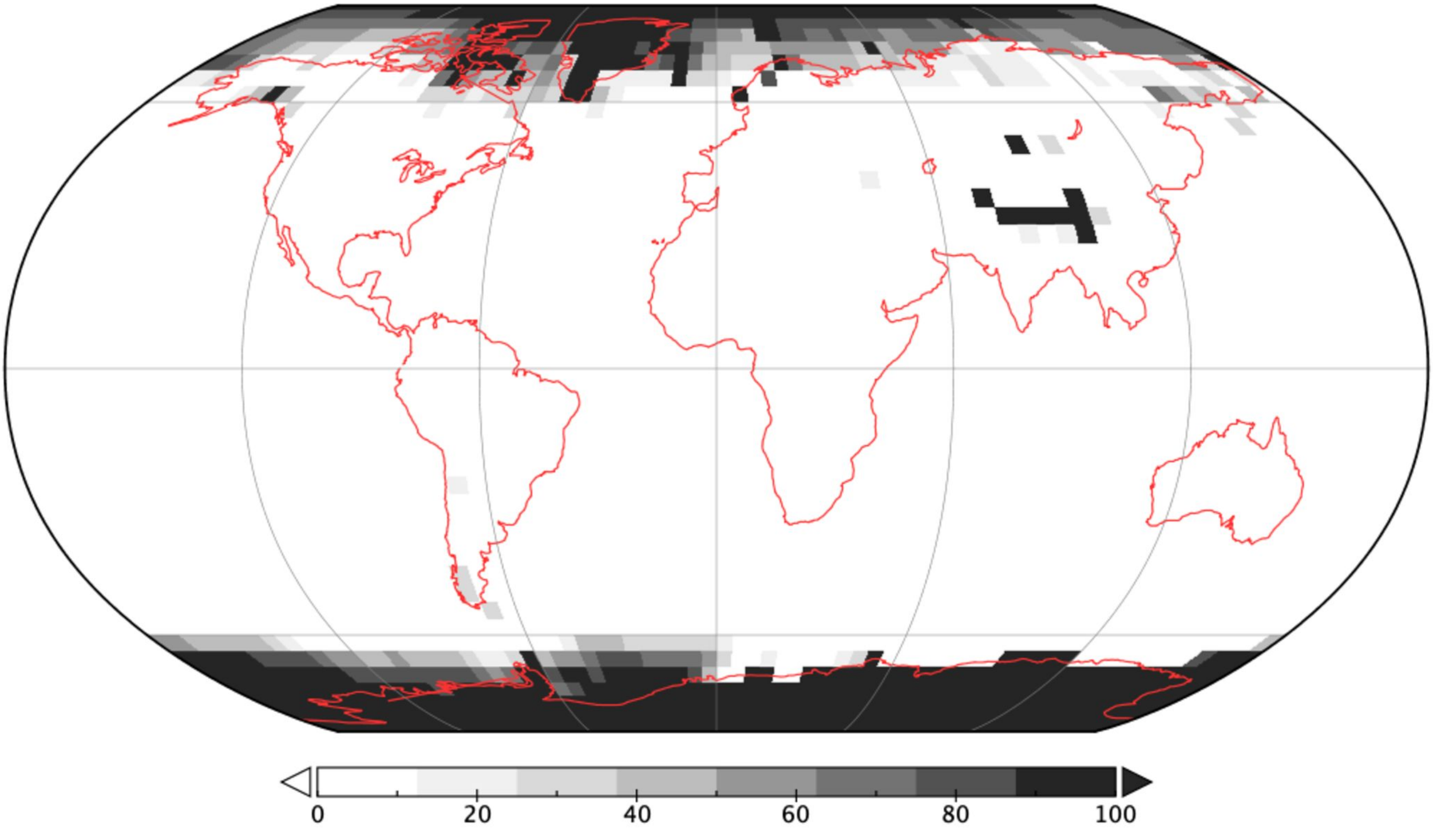

fig1d.png.

Simulation 04: Amasia_Rand_CTRL

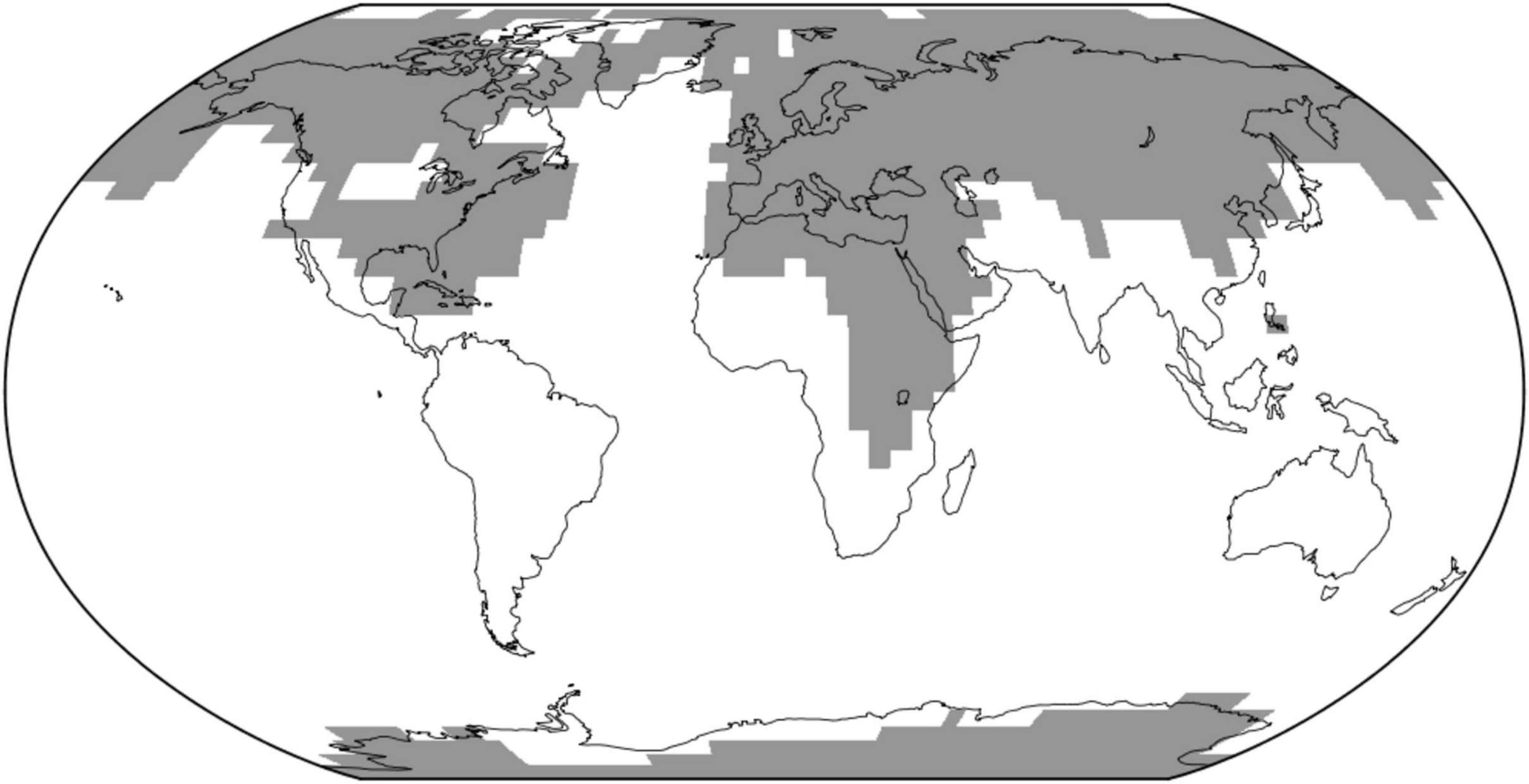

fig2b.png.

Simulation 05: Snow and ice coverage Dec/Jan/Feb

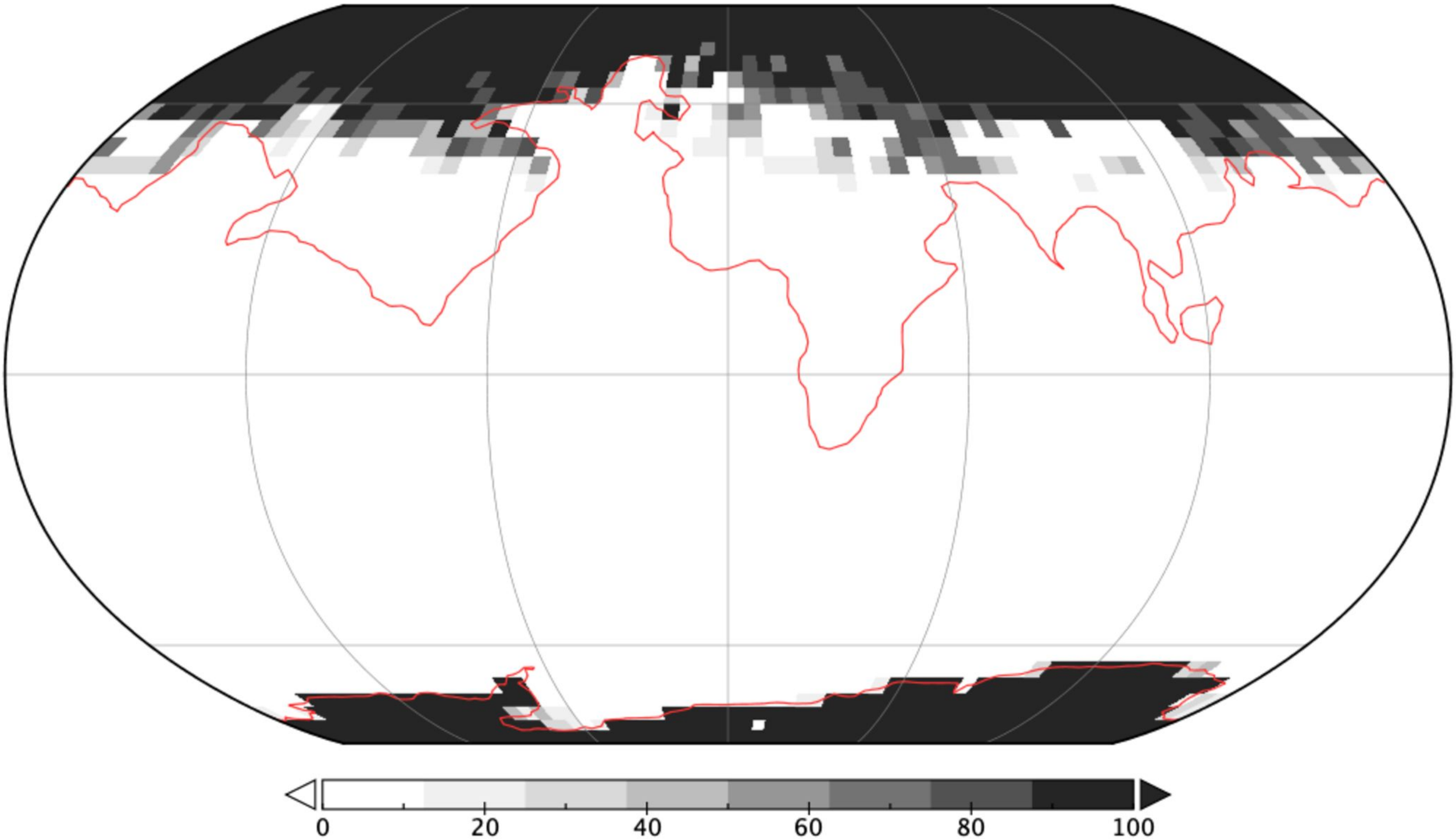

fig2c.png.

Simulation 07: Snow and ice coverage Dec/Jan/Feb

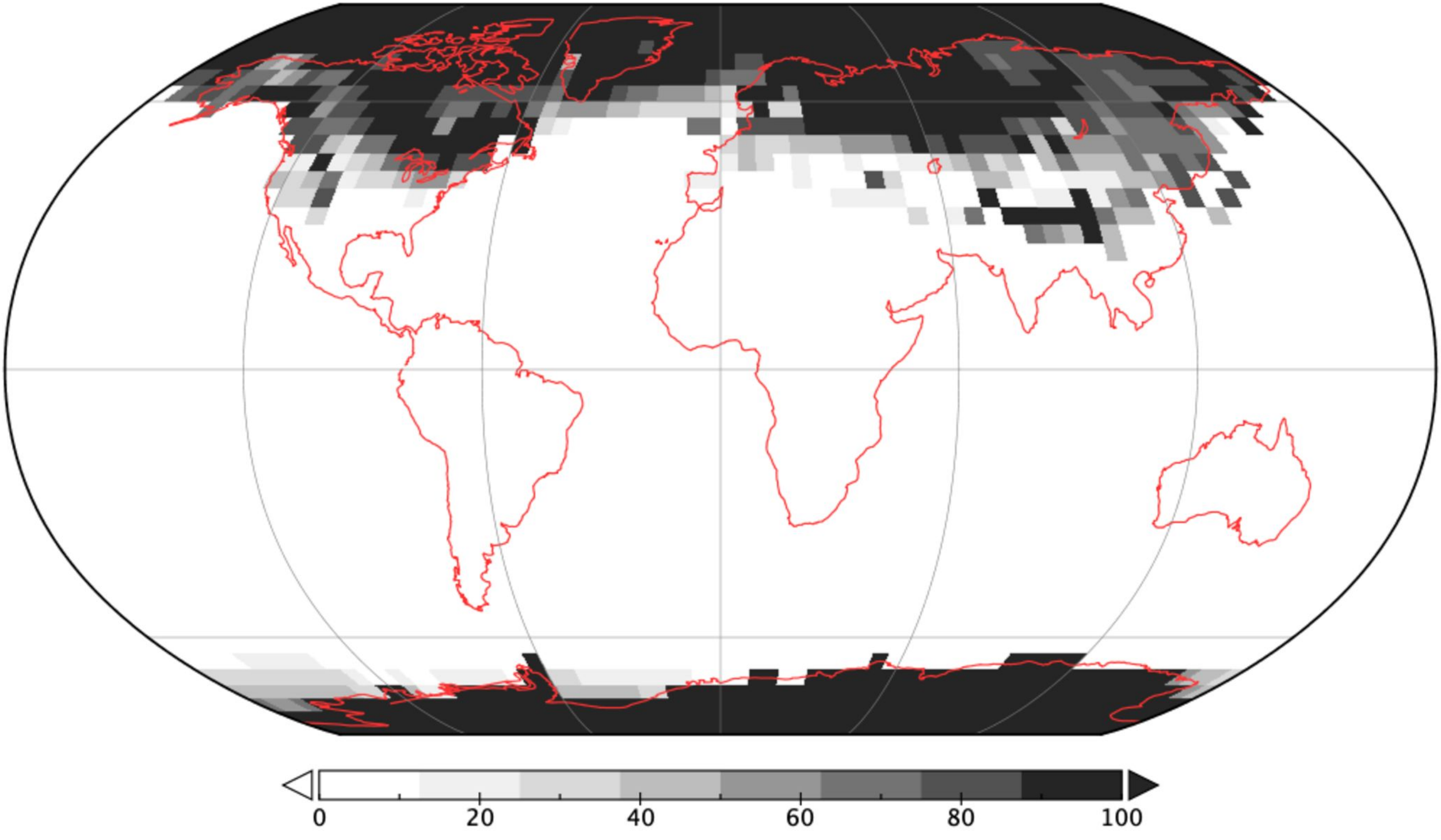

figS2c.png.

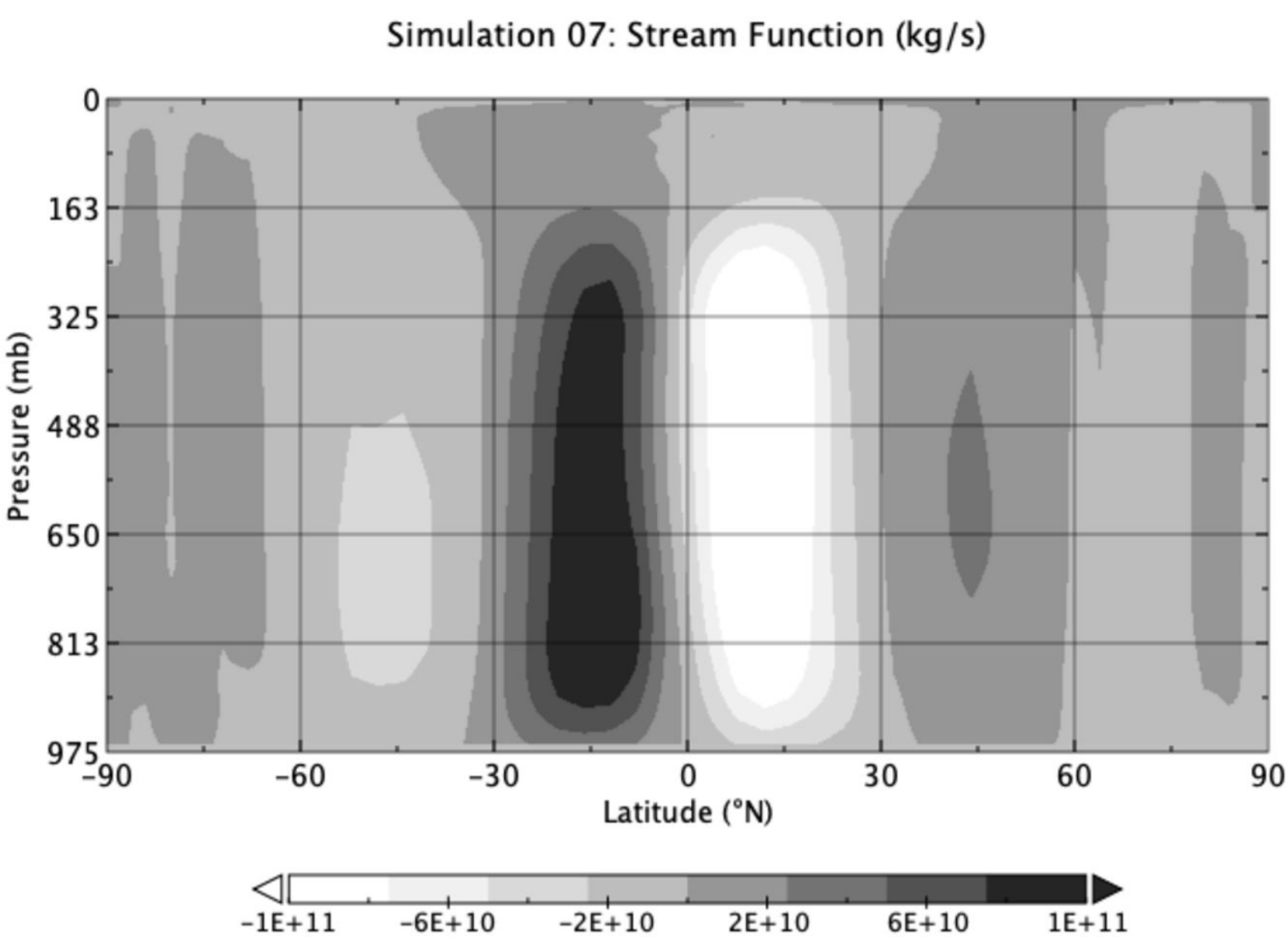
Simulation 07: Stream Function (kg/s)
Pressure (mb)
0
163
325
488
650
813
975
-90
-60
-30
0
30
60
90
Latitude (°N)
-1E+11
-6E+10
-2E+10
2E+10
6E+10
1E+11

fig1e.png.

Simulation 05: Amasia_Rand_PD

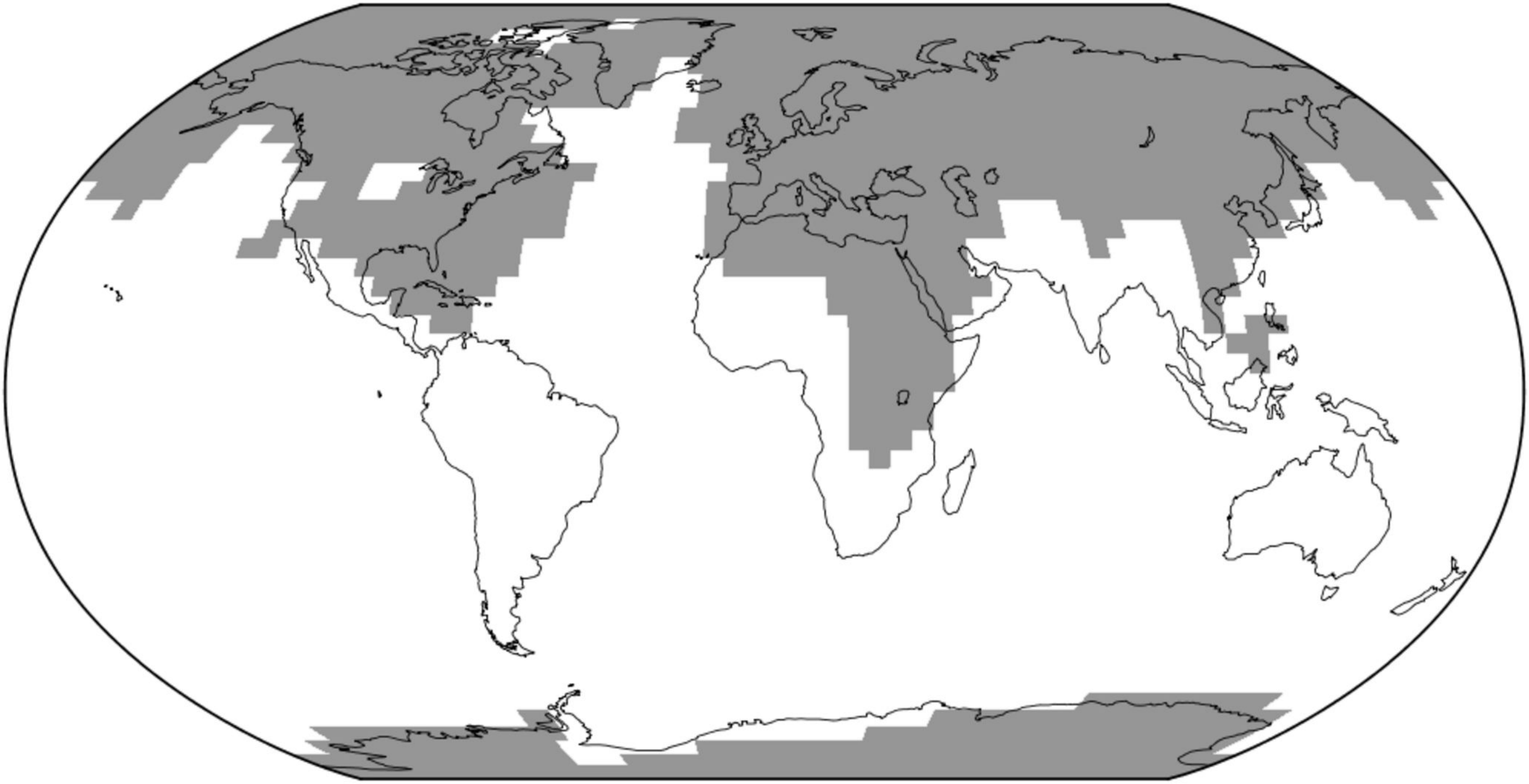

figS2a.png.

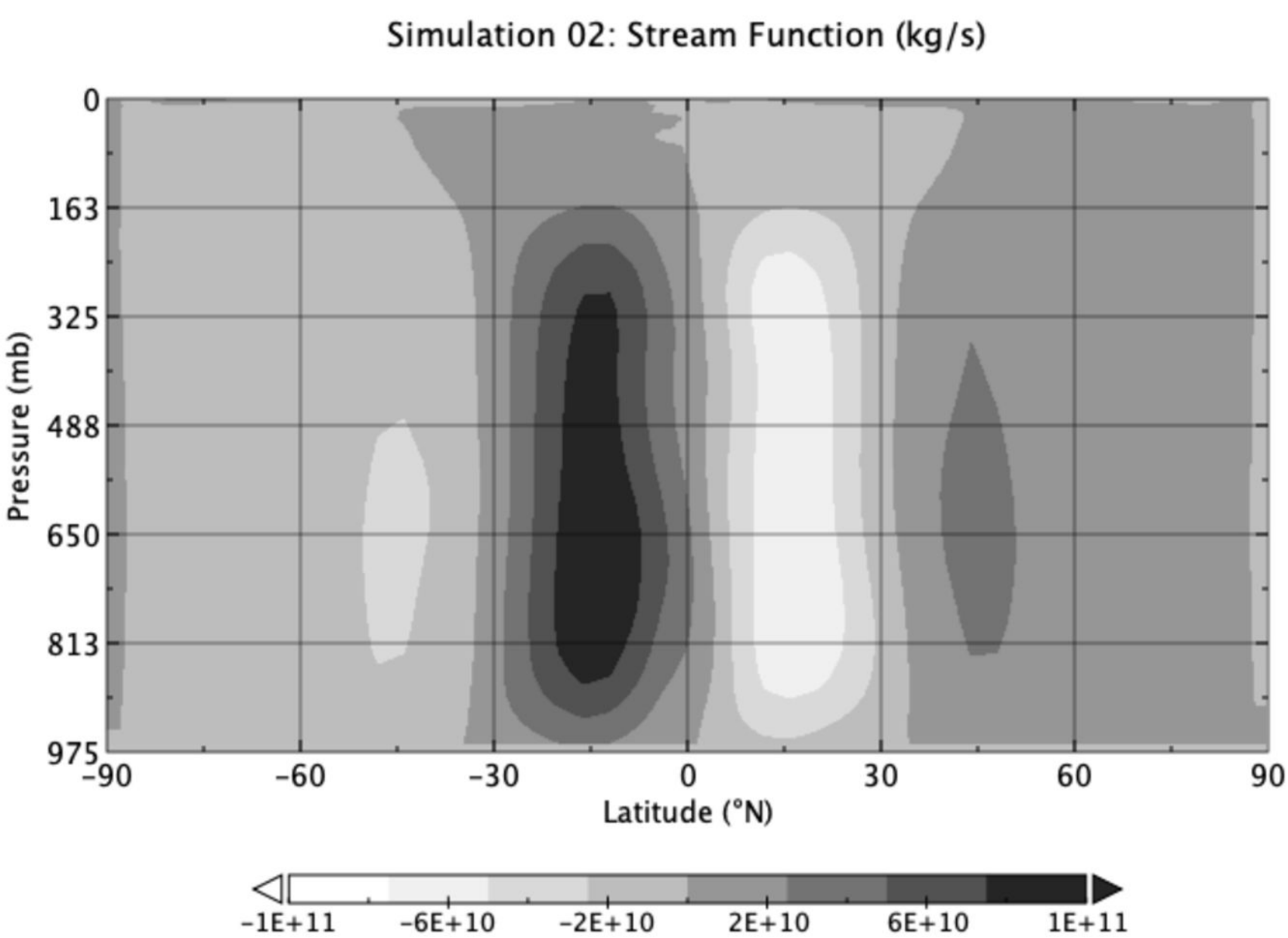
Simulation 02: Stream Function (kg/s)
Pressure (mb)
0
163
325
488
650
813
975
-90
-60
-30
0
30
60
90
Latitude (°N)
-1E+11
-6E+10
-2E+10
2E+10
6E+10
1E+11

fig1c.png.

Simulation 03: Aurica_250f

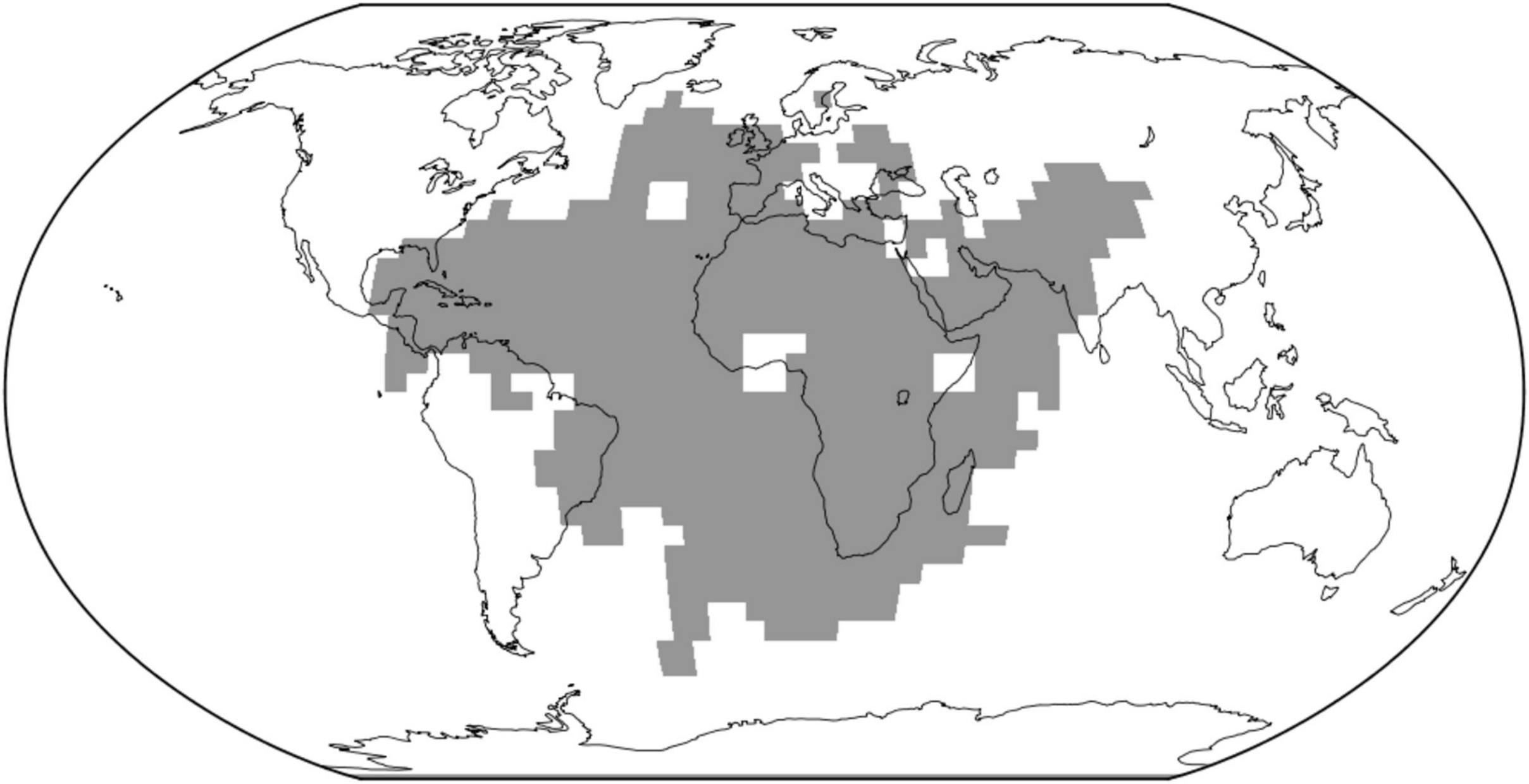

fig1f.png.

Simulation 06: Amasia_200f

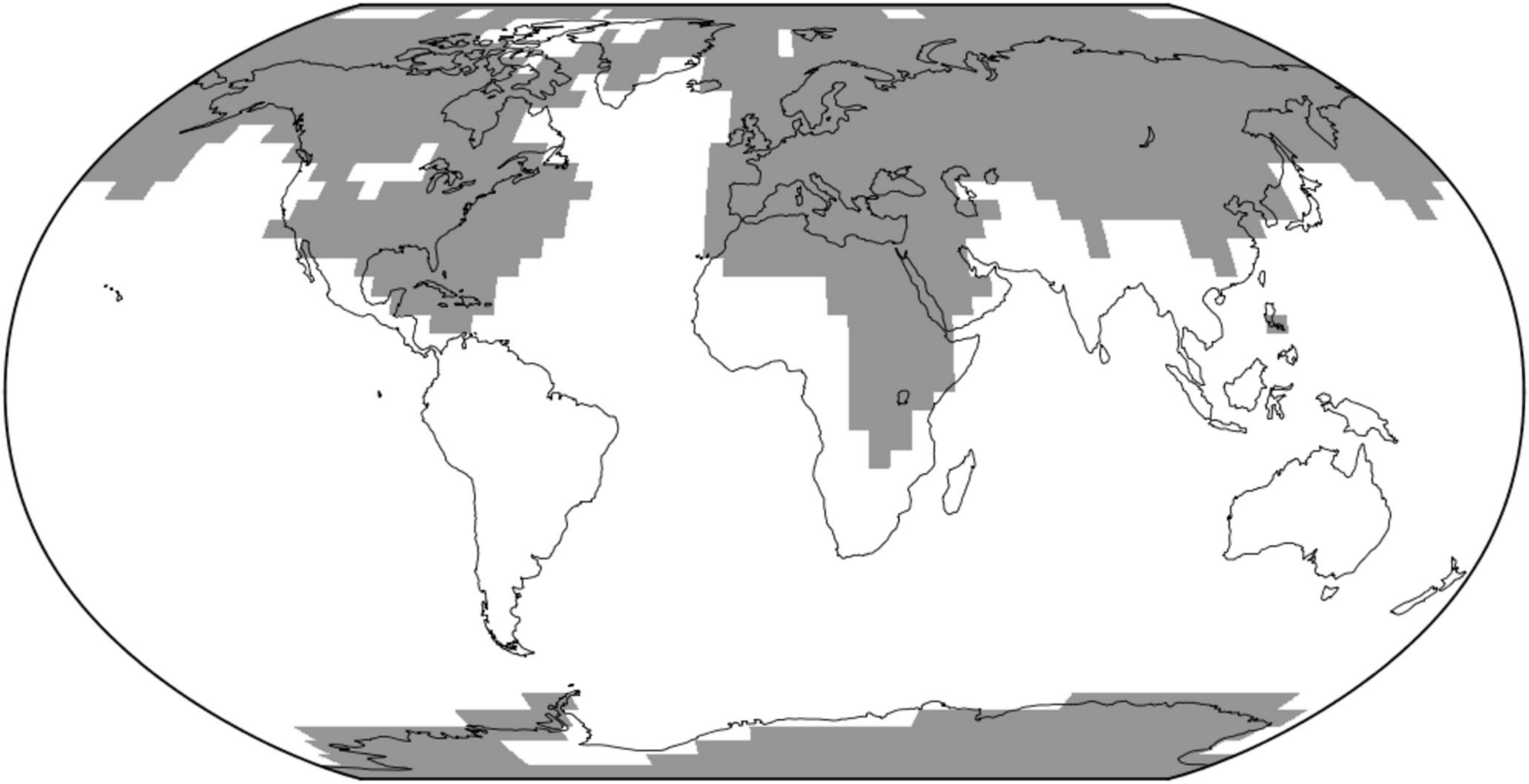

Figure 1a.

Simulation 01: Aurica_Rand_CTRL

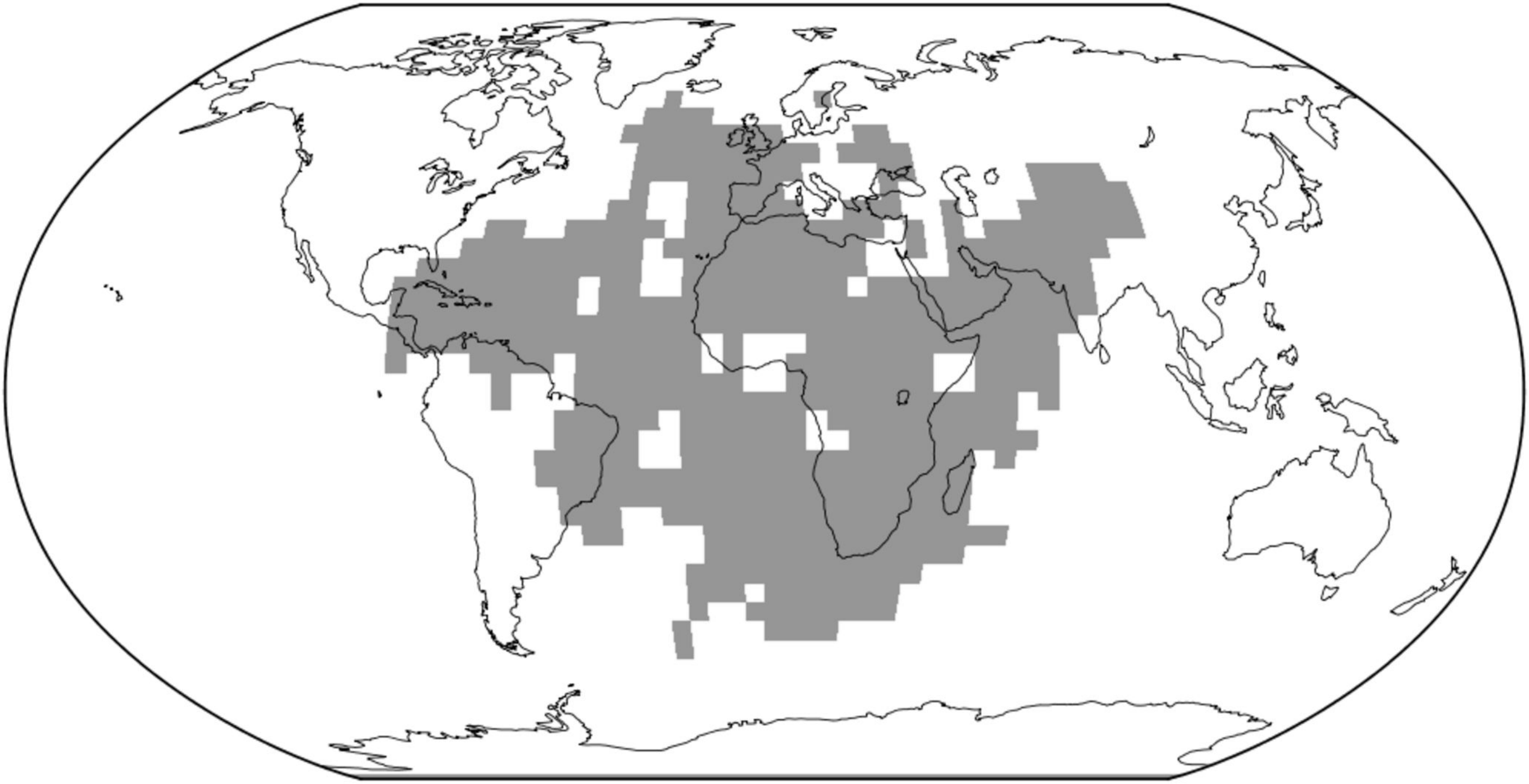

figS1.png.

Atmospheric Meridional Transport

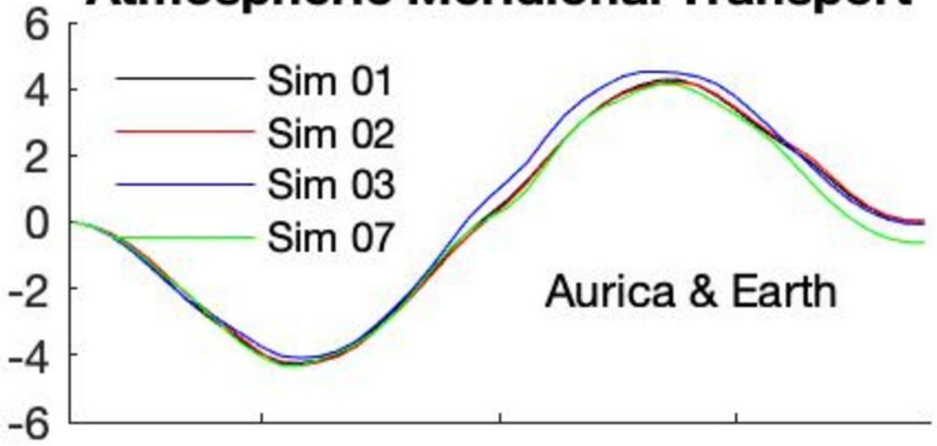

Atmospheric Meridional Transport

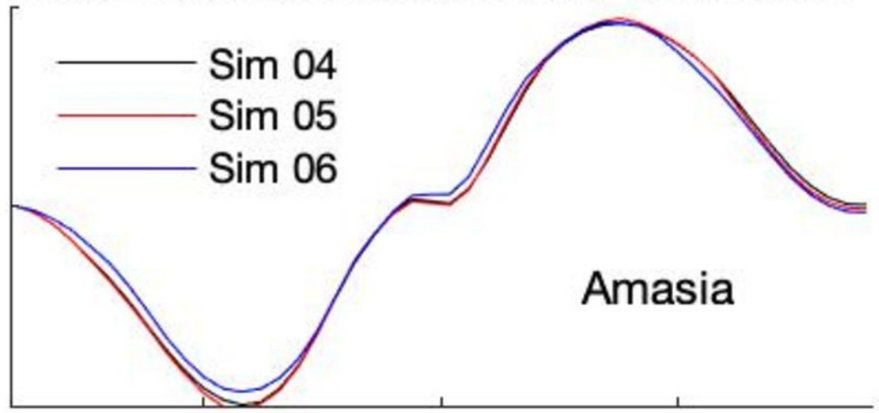

Oceanic Meridional Transport

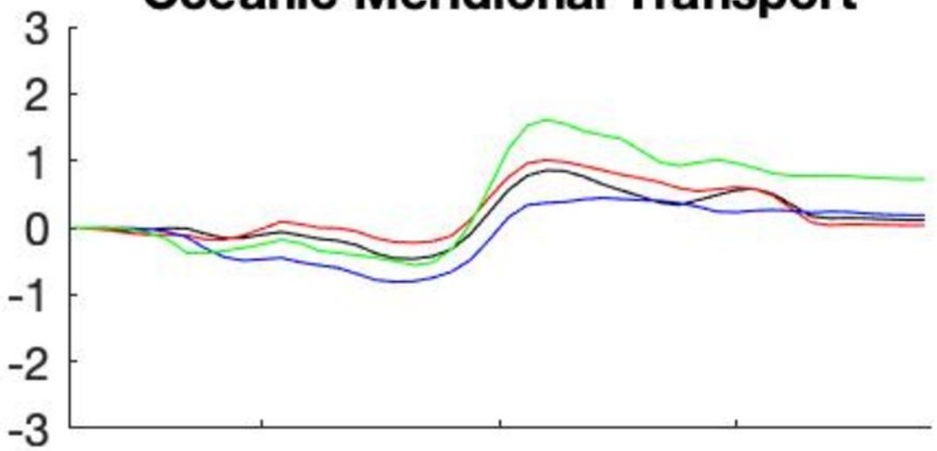

Oceanic Meridional Transport

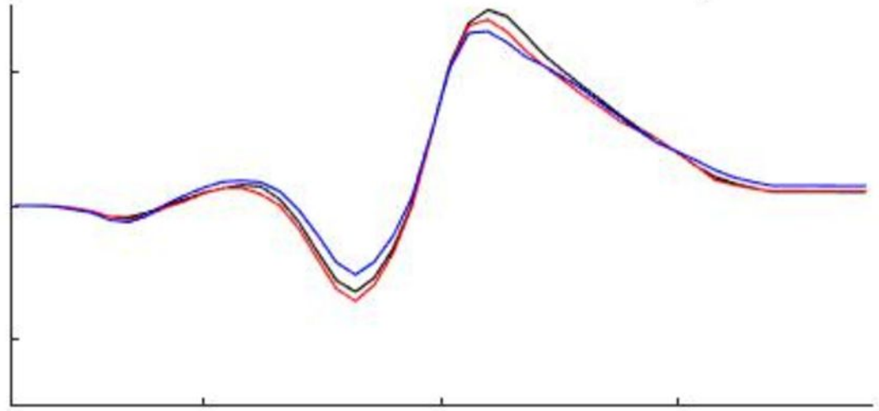

Total Meridional Transport

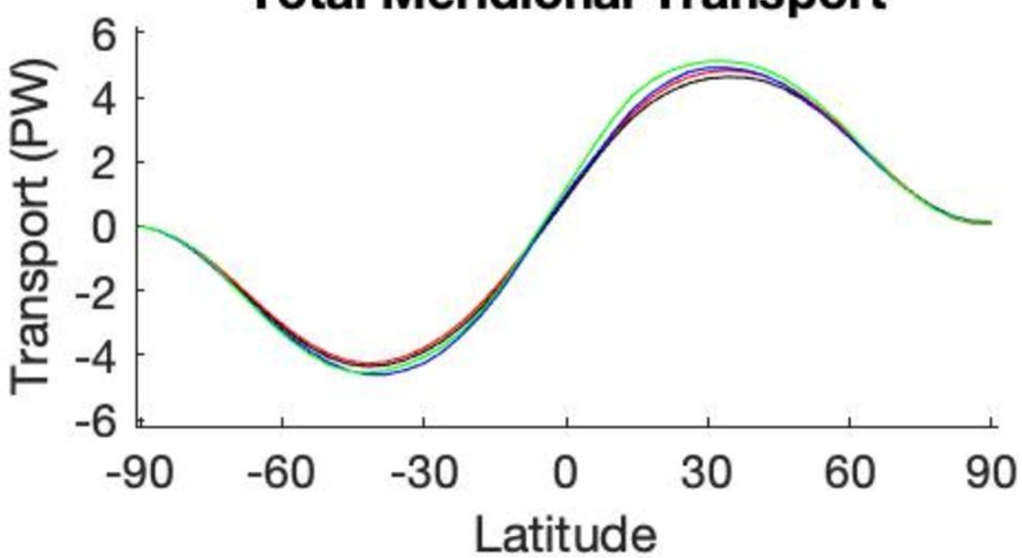

Total Meridional Transport

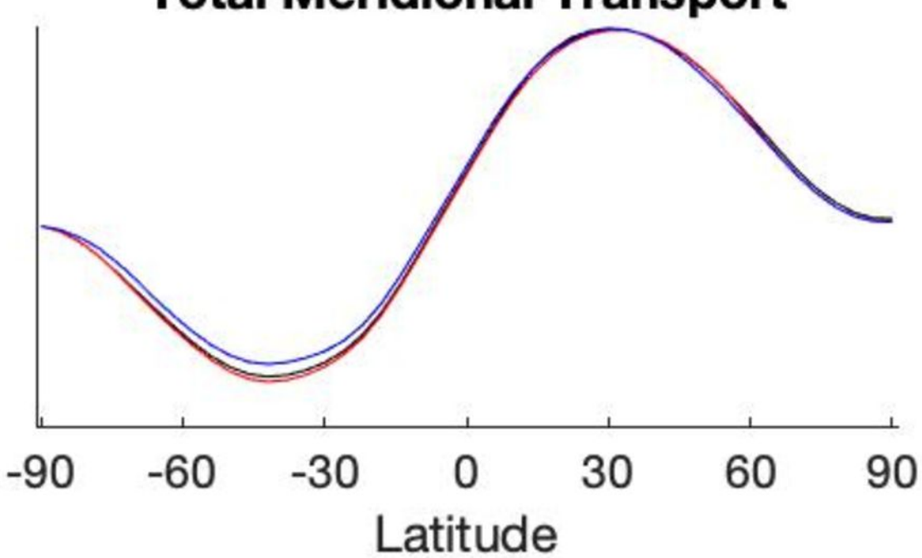

figS2b.png.

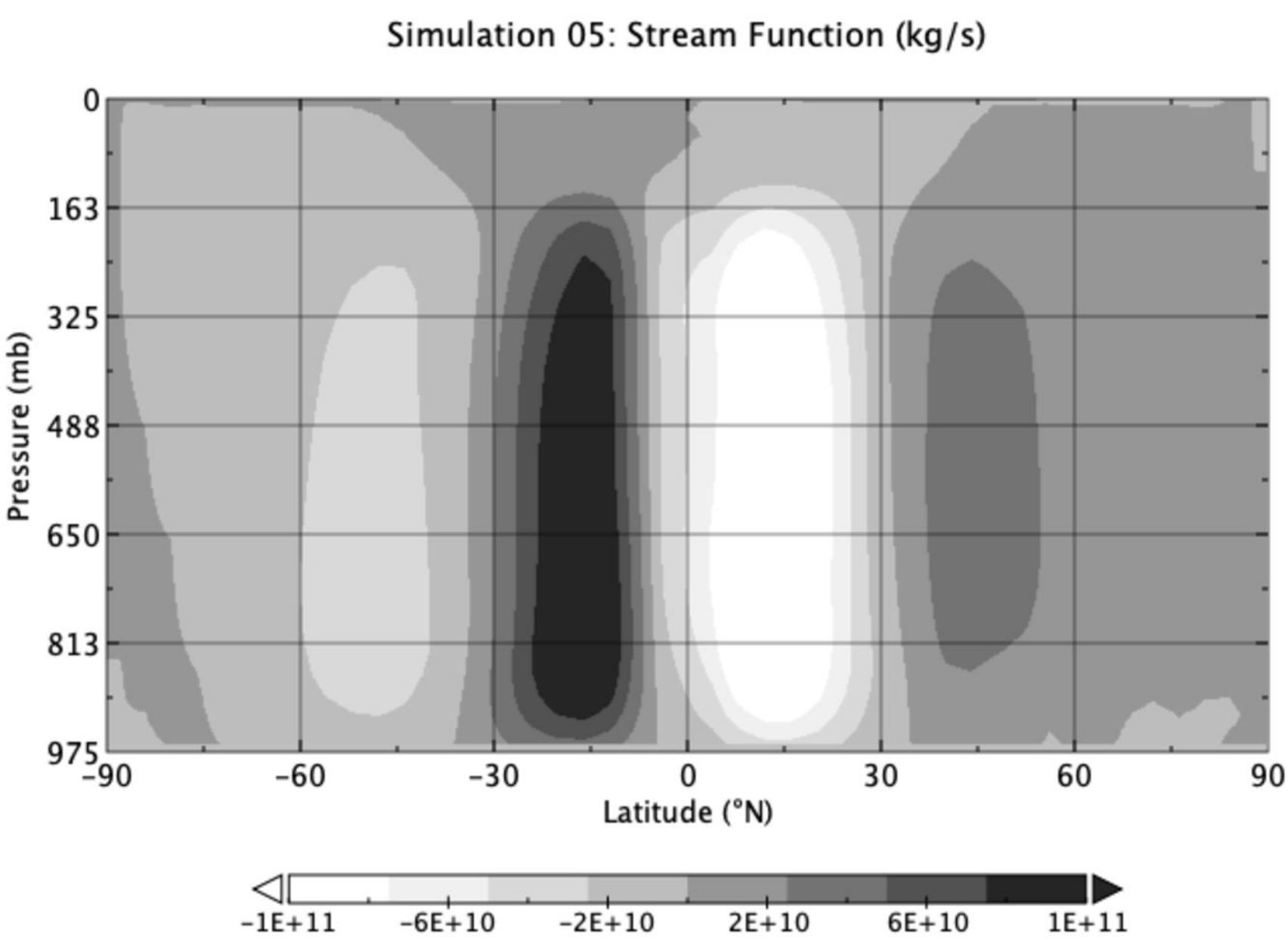
Simulation 05: Stream Function (kg/s)
Pressure (mb)
0
163
325
488
650
813
975
-90
-60
-30
0
30
60
90
Latitude (°N)
-1E+11
-6E+10
-2E+10
2E+10
6E+10
1E+11

fig2a.png.

Simulation 02: Snow and ice coverage Dec/Jan/Feb